Resource-Efficient Technologies 3 (2017) 422–428

Contents lists available at ScienceDirect

Resource-Efficient Technologies

journal homepage: www.elsevier.com/locate/reffit

Research paper

Ethanol steam reforming with Co^0 (111) for hydrogen and carbon nanofilament generation

Ashutosh Kumar[a] , Ram Prasad[b], Yogesh Chandra Sharma[a,*]

[a] Department of Chemistry, Indian Institute of Technology (BHU), Varanasi 221005, India
[b] Department of Chemical Engineering and Technology, Indian Institute of Technology (BHU), Varanasi 221005, India

ARTICLE INFO

Article history:
Received 6 February 2017
Revised 4 March 2017
Accepted 8 March 2017
Available online 19 April 2017

Keywords:
Catalyst deactivation
Characterization
ESR
Hydrogen production

ABSTRACT

The cobalt metal catalysts are highly active at low temperature ESR. In this study, ESR was studied over barren Co metal (Co^0) from oxalate precursor without any pre-reduction to find out its role in hydrogen and carbon nano-filament generation. The ethanol conversion was found to be 100% with 96.5% hydrogen selectivity at 723K. The time on stream (TOS) study has shown stability up to 19h for Co catalyst. The diameter of Co-carbon nanofilament was calculated and found to be typically in the range of 70–80 nm by the TEM image analysis of spent catalyst. The SEM with EDS analysis revealed that Co^0 state was found in between the carbon nanofilament as well as at the tip of carbon nanofilament. The obtained Co-C nanofilament displayed an adsorption capacity of 552 mg/g at optimum parameter of pH = 2, contact time = 60 minute, concentration = 30 ppm, dose = 0.05g for Orange G dye removal without any chemical or physical treatment. This approach has shown significant results in terms of hydrogen generation and method of Co carbon nanofilament for further utilization in different prospects.

1. Introduction

Energy demands and water pollution are always universal issues in front of the world. The resource's requirement in the world is increasing day by day to meet the energy and water demands of the population. The resources are inadequate for enormously increasing population and so it needs proper planning for water resources [1]. The water quality with land use prospective studies suggests that urbanization leads to increment of pollution load over fresh water holy river Ganga rather than agriculture [2]. Urbanization cannot be stopped but sustained. Hence, the recycling of waste or use of resources in a cyclic manner has a greater consequence in upcoming days. Near future assessment of prerequisite energy suggests opting hydrogen as a best one among renewable energy carriers. One of the potential methods for hydrogen generation is steam reforming process [3–5]. Among which utilization of renewable sources ethanol is the best feedstock because it is nontoxic and renewable. The work of George et al. suggests and enlightens the possibilities of using integrated steam reformer with Polymer Electrolyte Membrane Fuel Cell (PEMFC). However, the cost-effective catalyst must be needed during ethanol steam reforming because it has significance in overall cost of hydrogen. Therefore, non-noble metal based catalyst can be a sustainable option [6]. Literature survey suggests that among non-noble metal, Co and Ni based catalysts have shown better C-C bond scission ability as compared to other metal catalysts. Furthermore, between Co and Ni, Co has better efficiency at lower temperature (673K-773K) than Ni. Except, few noble metal catalyst most of the catalysts suffered from deactivation due to carbonaceous deposition during ESR.

The different phase stability and activity suggest that Co is not only highly active for ethanol steam reforming (ESR) in its metallic form but also a major contributor for carbon deposition [7,8]. Co^{2+} and Co^0 states are also active in acetaldehyde as well as ethanol steam reforming [9,10]. Yue et al. suggested that addition of Co in the Ni metal catalyst alloy is able to reduce the carbon deposition during ESR [11]. Among non-noble metal catalysts, cobalt based catalyst with various supports was used by several authors for ethanol steam reforming (ESR) process [12–21]. This reveals that cobalt is highly active for ESR especially at 753K. However, carbonaceous deposition is a great issue regarding catalyst stability. Different cobalt precursors have also significant contribution in carbon deposition at catalyst surface. The effect of different precursors over carbon deposition was reported by Song et al. with

* Corresponding author. Department of Chemistry, Indian Institute of Technology (BHU), Varanasi 221005, India. Tel.: +91 542 6702865; fax: +91 542 670 2876.
E-mail address: ysharma.apc@iitbhu.ac.in (Y.C. Sharma).

https://doi.org/10.1016/j.reffit.2017.03.006

nitrate, chloride, sulphate, acetate, octacarbonyl, carbonate, acetyl acetonate and oxalate, but ESR performances were not reported with cobalt oxalate precursor [22]. One objectionable point was the use of ethanol as an impregnation medium for each precursor to impregnate over CeO_2. Because the cobalt oxalate precursor is insoluble in ethanol, it is not a good impregnation medium for the aforementioned precursor. Cobalt oxalate is soluble in ammonia solution, and so it can be used as an impregnated medium for better distribution of active metals.

Orange G is an azo dye used by several dye industries. It contains a colour producing azo (-N=N-) group and others having higher affinity towards fibres and water auxochromes (-SO_3,-OH etc) group. Azo dye is largely used (70%) group among all dyes globally [23]. The dye is carcinogenic, affects water vegetation and is reported to be non-biodegradable [24]. Several approaches of dye removal from waste water through adsorption with carbon are comparatively cheaper. Adsorption of Orange G over carbon shows transfer of the dye from liquid to a solid medium. However, it needs further disposal but oxidation of this dye with carbon at higher temperature or photo degradation in non-harmful form is a sustainable alternative.

The literature survey suggests that metallic cobalt phase is active for C-C bond scission but it also contributes for carbon filament formation [25–27]. The significant property of cobalt oxalate is that in situ thermal treatment in inert atmosphere at 673K typically forms cobalt metallic phase [28]. There is no need to pre-reduce the catalyst to be in active phase and with little support Co needs promoter to be reduced in metallic phase completely [29]. However, Tuti and Pepe worked over barren Co metallic catalyst by pre-reducing Co_3O_4 catalyst. The time on stream study and carbon formation study were also not testified [30]. Therefore, cobalt oxalate precursor was used first time in ESR as a catalyst for in situ formation of cobalt metal through thermal decomposition without any prereduction or chemical treatment. This method reduces the cost for reduction of Co_3O_4 into Co in metallic state. The study about filamentous carbon formation during ESR is still under study. Few authors had suggested the tip growth phenomenon occurs during ESR, whereas, few contradicted this mechanism [31–33]. Therefore, the study over barren active cobalt metal gives new insight of this probable mechanism. Moreover, first time the waste generated after ESR as a mixture of carbon and catalyst was used for the dye (Orange G) abatement.

2. Experimental

The experiment was performed in two stages. First of all ethanol steam reforming was performed for 31h continuously. At the next stage, catalyst with carbonaceous deposition (Co + Carbon) was used for waste water treatment.

2.1. Catalyst preparation

Analytical reagent grade cobalt (II) oxalate dihydrate ($CoC_2O_4.2H_2O$) precursor was used for active Co catalyst preparation. The cobalt metal catalyst was thermally prepared from $CoC_2O_4.2H_2O$ precursor in inert atmosphere at 773K. The $CoC_2O_4.2H_2O$ (5g) was kept in a tubular reactor and N_2 gas was continuously fed (10 ml/min) from room temperature. The temperature was increased at the rate of 20K/min up to 773K and subsequently thermal treatment was continued for 1h. After 1h the catalyst bed was cooled in N_2 atmosphere up to room temperature and the formed Co metal was collected for further characterization and experimentation.

2.2. ESR performance

ESR was performed at atmospheric pressure with cobalt catalyst (500 mg) in a fixed bed flowed quartz tubular vertical reactor having length 40 cm and inner diameter of 3.2 cm. Ahead of reactor, the preheater was assembled to evaporate the ethanol and water mixture (molar ratio = 3:1) fed with the help of syringe pump at the rate of 4 ml/hr. The ESR was performed in 573K–923K range with 50K temperature interval. The time on stream performance was done at 723K reaction temperature, since it was found as a best optimum temperature. The concentration of gaseous mixture was analysed with an online Thermo scientific Trace 1110 gas chromatogram equipped with thermal conductivity detector and flame ionization detector with methanizer. The Porapack Q column (80–100 mesh size) was used for the analysis of liquid mixture residue and hydrocarbon gaseous mixture (CO, CO_2, CH_4, CH_3CHO, H_2O, C_2H_5OH, C_2H_2 and C_4H_{10}). Hydrogen gas was analysed in Molecular sieve column. The selectivity of gases, yield of hydrogen and conversion were calculated by following expressions [34]:

$$H_2\ yield\ (\%) = \frac{moles\ of\ H_2\ produced\ by\ ESR}{moles\ of\ ethanol\ fed \times 6} \times 100$$

$$X_{reactant}\ (\%) = \frac{F_{reactant\ in} - F_{reactant\ out}}{F_{reactant\ in}} \times 100$$

$$Selectivity\ of\ product\ Y\ (\%) = \frac{N \times moles\ of\ Y\ produced}{2 \times moles\ of\ ethanol\ converted} \times 100$$

$$Selectivity\ of\ H_2\ (\%) = \frac{N \times moles\ of\ H_2\ produced}{[3 \times (F_{ethanol\ in} - F_{ethanol\ out}) + (F_{water\ in} - F_{water\ out})} \times 100$$

After ESR performance N_2 was flushed for 30 minutes to remove the (ethanol–water mixture) vaporized feed mixture.

2.3. Orange G dye removal performance

The chemicals used, NaOH, HCl and Orange G ($C_{16}H_{10}N_2Na_2O_7S_2$) dye were purchased from Merck, India, with analytical grade purity. The coloured dye was stable within the pH range of study. The stock solution (100 mg/l) of Orange G dye was prepared and further lower concentration of solution was prepared by dilution. The batch experiment was performed to find out the adsorption efficiency of cobalt carbon mixture at different variables (pH, dose, concentration and time). The batch experiment was performed in100 mL reagent bottles by known concentration of 50 mL dye, pH and a requisite dose of the adsorbent. The mixture was stirred up by using water bath shaker with agitation speed of 90 rpm at 30° C. Samples were taken out at particular time interval and supernatants were centrifuged at 10000 rpm for 10 min. Afterwards, the concentration of dye was analysed on the Shimadzu spectrophotometer (UV-1800) at $\lambda_{max} = 480$ nm for residual concentration determination of the dye. Percentage removal of adsorbate (Orange G) was calculated by following expression [35]:

$$\text{Removal of Orange G}\ (\%) = \frac{(C_i - C_e)}{C_i} \times 100$$

Where, C_i and C_e are the initial and equilibrium concentrations of Orange G.

2.4. Catalyst characterization

Powder High resolution X-ray diffraction (HR-XRD) patterns of the fresh and spent Co catalysts were collected using a Bruker D8

instrument equipped with a Cu Kα radiation (λ = 0.154 nm). The data were recorded between 20° to 80° 2θ, at a step width of 0.02° and accounting time of 10s per point.

The analysis of particle size and morphology of catalyst and spent catalyst were done by SEM (Scanning Electron Microscopy)–EDS (Energy Dispersive Spectroscopy) and TEM (Transmission Electron Microscope). SEM-EDS was recorded on ZEISS EVO 18 SEM coating of quorum Q150R ES having model number 51-ADD0048, and TEM image was recorded on Fei TECNAI 200 Kv.

Specific surface area and pore volume were analysed from smart sorb 92/93 surface area analyser using nitrogen physisorption at liquid nitrogen temperature.

3. Result and discussion

3.1. Characterization studies

Surface area of Co metal was found 3.93 m^2/g but after reaction the surface area of cobalt with carbon increases to 108.12 m^2/g. The pore volume was also found higher for cobalt with carbonaceous mixture. This is due to presence of nano carbon filament formed during ESR reaction (Table 1).

The cubic and face-centred crystallite of Co peak at 2θ value 44.20°, 51.53° and 75.87° was matched with JCPDS (89–4307) with assigned plane (111) (200) (220) respectively. Whereas, the 2θ value 36.47° (111), 42.41° (200), 61.47° (220), 73.62° (311) and 77.49° (222) were found corresponding to JCPDS (71–1178) of CoO. Moreover, the intensity of Co peaks of each plane can be observed higher from Fig. 1 comparative to the peak intensity of CoO. The planes (111), (200) and (220) were observed common in both phases of Cobalt. The intensity of (111) plane was found highest as compared to other planes for Co^0 phase, whereas, intensity of (111) and (200) planes are comparative to CoO state of cobalt. Overall, (111) plane was predominantly formed on the cobalt catalyst. The Rietveld refinement was performed for both phases of cobalt. The in situ formation of Co and CoO was also supported by the EDS analysis of catalyst as shown in Fig. 2. It shows highly intense peaks of Co with very less intense peaks of oxygen which indicates significant amount of Co^0 formation as compared to CoO. The unmarked peaks in EDS graph were copper because of the use of copper grid for sample preparation. The crystallite size calculated were found as 19 nm, 22.34 nm and 26.10 nm, whereas, the particle size calculated with the help of image-J software was found in the range of 500–600 nm. The larger particle size suggests agglomeration due to in-situ thermal treatment process.

3.2. ESR performance test

The selectivity of gaseous products generated and ethanol conversion during ESR were shown in Table 2. The ethanol conversion was completed at temp 723K. The selectivity of H_2 and CO_2 was found highest at 723K. The CH_4 selectivity was reduced with increasing temperature, whereas, CO selectivity was increasing at higher temperature. It may have occurred due to decomposition of ethanol at higher temperature. It was also interesting that at temperature higher than 723K, water formation started. At temperature 773K and 823K CH_4 selectivity was higher and water formation was also higher, which suggests the hydrogenolysis of ethanol

Table 1
Surface area and pore volume of catalyst and spent catalyst.

Sample	Surface area (m^2/g)	Pore volume (ml/g)
Co catalyst	3.93	0.0037
Carbon + Co	108.12	0.1602

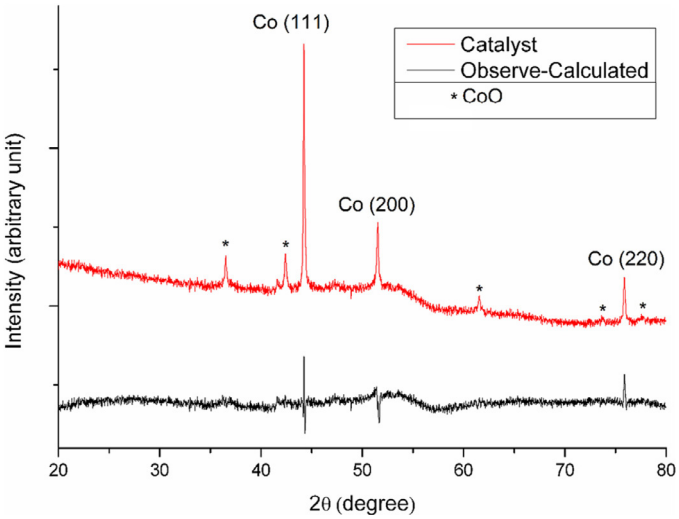

Fig. 1. X-rays pattern of Co catalyst.

can be a dominant reaction. The bar graph (Fig. 3) of $H_2/EtOH_{in}$ (3.5 mol) at different temperatures also suggests that 723K is the optimum temperature to generate hydrogen. The acetaldehyde selectivity was only found at temperature lower than 673K. Comparison of literature survey with this study suggests that by using support, the optimum temperature in terms of hydrogen selectivity is in agreement with Passos et al. [10]. Garbarino et al. have also performed the ESR with Co nano-particles and found maximum hydrogen selectivity at 773K but they performed the experiment at an interval of 100K and that is the reason that they escaped the temperature 723K [13], which can be an optimum temperature. Moreover, by using few supports with Co the optimum temperature for hydrogen selectivity is increased but carbon formation decreased [8,14,27]. The selectivity of constituent gas also varies by using different kinds of support, because of divergence in reaction pathway selection [29].

The 21 h time on stream data (TOS) with selectivity of different gaseous products during ESR was shown in Fig. 4. Initially up to 8h, the mixture of generated gas contains H_2, CH_4, CO_2 and CO and after it, the C_4H_{10} was also found in outlet gas mixture with very less selectivity. Up to 17h, the generated gaseous products were not significantly varied, but after the selectivity of H_2 and CO_2 both lowers down and the selectivity of CO and CH_4 was increased abruptly. This behaviour suggests the generation of CH_4 at the cost of CO_2 and H_2. The Co and carbon mixture and yield of carbon were found to be 7.76g and 44.88%, respectively, after 21 h TOS reaction.

After performing ESR, the catalyst with carbon was characterized with SEM-EDS, HR-XRD and HR-TEM, which have been shown in Figs 5–7 respectively. The images confirm a number of carbon

Table 2
Catalyst activity of Co for ESR (molar ratio of $H_2O:C_2H_5OH = 3:1$, WHSV = 5.244h^{-1}).

Temp(K) (%)	Ethanol conversion	Selectivity (%)				
		H_2	CO	CH_4	CO_2	CH_3CHO
573	52	26.7	6.4	14.1	7.3	28.3
623	82	44.4	29.6	12.9	14.6	11.7
673	100	81.5	5.7	13.9	22.5	0
723	100	96.5	6.1	3.2	27.6	0
773	100	89.7	7.4	10.1	26.9	0
823	100	79.0	15.0	17.45	26.5	0
873	100	72.3	25.2	9.1	21.6	0
923	100	64.9	43.2	9.0	21.0	0

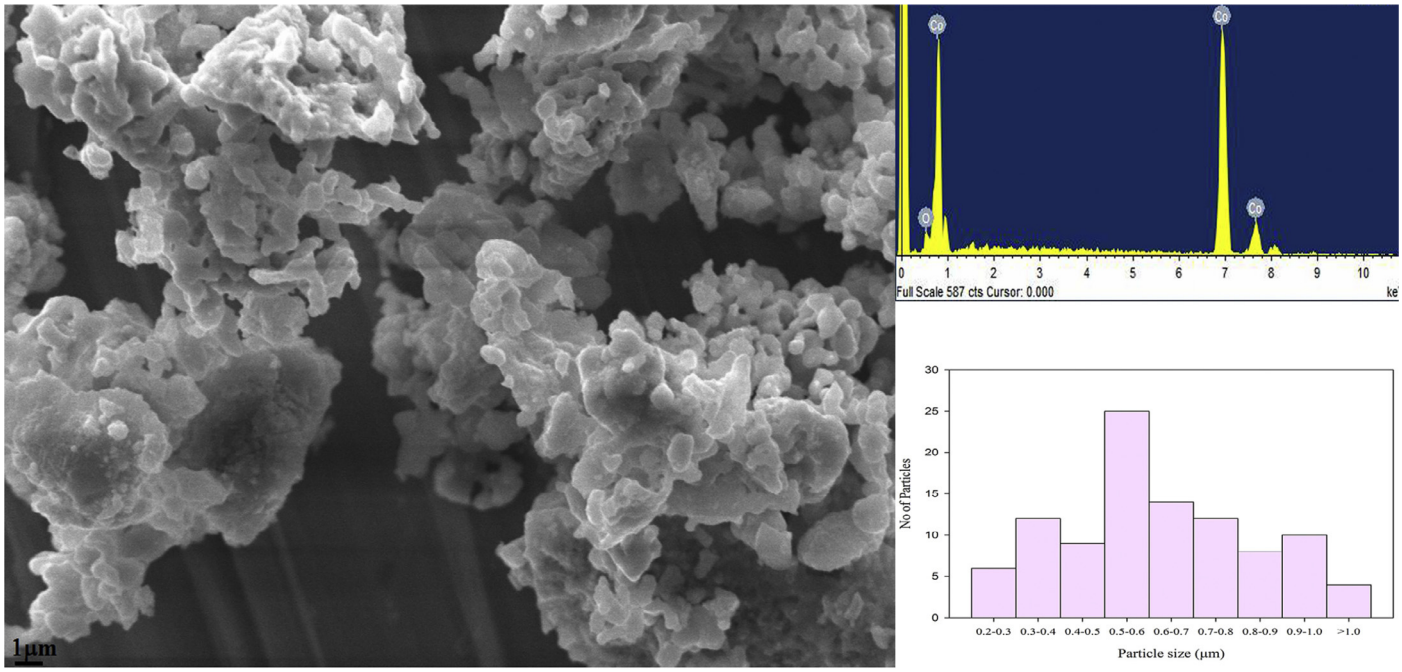

Fig. 2. SEM image and EDS of Co catalyst.

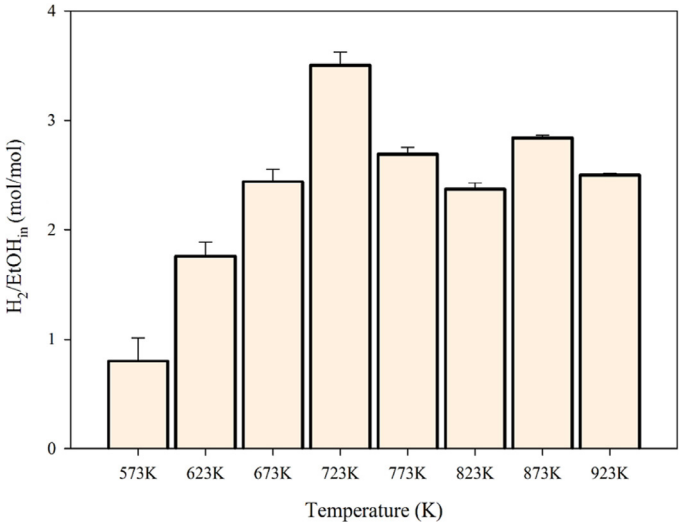

Fig. 3. Number of mole of hydrogen per mole ethanol with temperature.

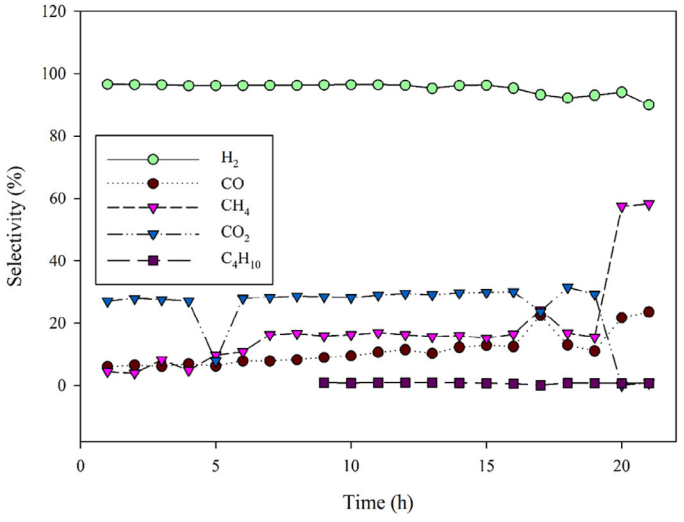

Fig. 4. Selectivity of gaseous products of ESR on Co catalyst at 723K plotted against time on stream (Temperature = 723K, Time = 21h, molar ratio of H_2O:C_2H_5OH = 3:1, WHSV = 5.244h^{-1}).

filament formations during ESR. On the basis of the gaseous products formed during reaction, the most probable reaction to generate carbon can be considered either decomposition of CH_4 and CO (eq1 and eq2) or hydrogenation of CO and CO_2 (eq3 and eq4). However, the CH_4 decomposition occurred at higher temperature (>1173K) [36]. The Boudouard reaction is sensitive upon step edge of catalytic surfaces [37]. Besides these two aforementioned reactions, the hydrogenation reaction may be the most favourable reaction for carbon deposition.

$$CH_4 \leftrightarrow 2H_2 + C \quad (1)$$

$$2CO \leftrightarrow CO_2 + C \quad (2)$$

$$CO + H_2 \leftrightarrow H_2O + C \quad (3)$$

$$CO_2 + 2H_2 \leftrightarrow 2H_2O + C \quad (4)$$

The growth of carbon filament after reaction and presence of cobalt at the tip of filament support the tip growth phenomenon during ESR. However, during EDS analysis the cobalt metal was not only found at the tip of filament but also in between the filament. The TEM image analysis also shows filamentous carbon with number of branches initiating from a common point. The carbon nanofilament diameter calculated from image J software was found in between 70 and 80 nm. However, from SEM image, few carbon filaments with larger diameter can be observed due to agglomerated form. It is also interesting that after reaction, the size of Co get reduced and more homogenized with carbon formed during ESR. The HR-XRD of spent catalyst has not any single peak of CoO phase, whereas all of the 3 planes of Co^0 existed predominantly. The absence of CoO phase indicates the reduction of CoO into Co during the reaction or small concentration of it get involved in carbon filament formation. On further, HR-TEM image analysis of carbon nanofilament indicates the contribution of (111) and (200)

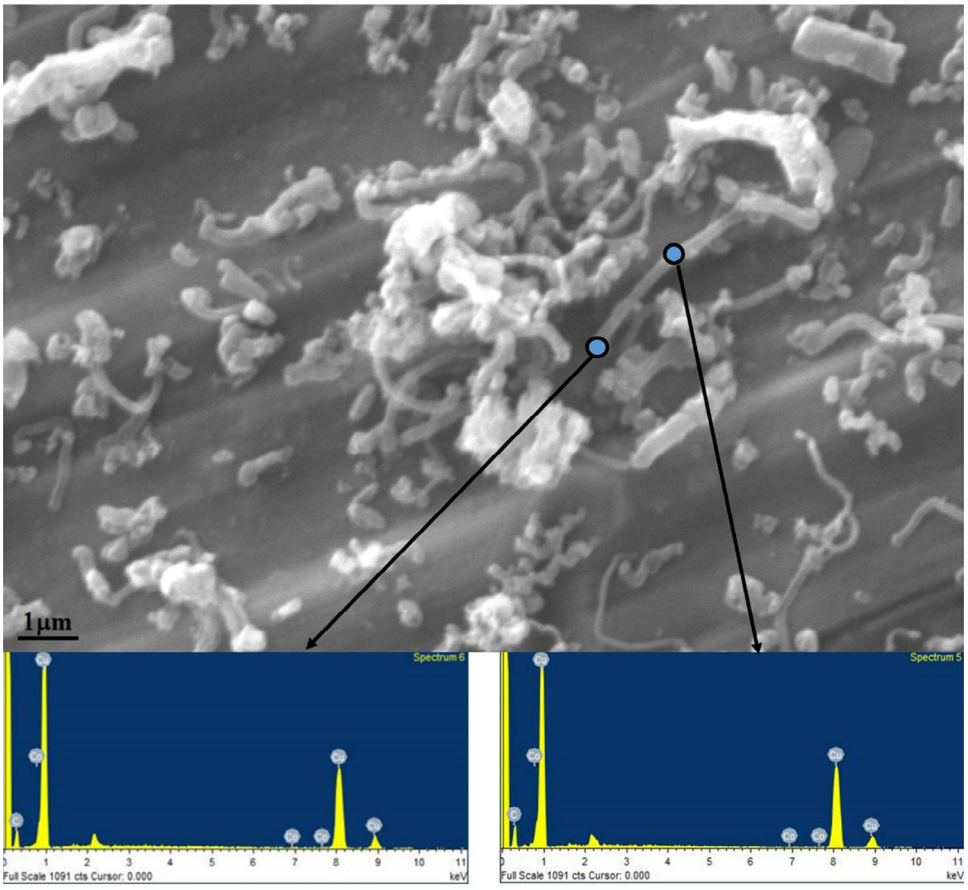

Fig. 5. SEM-EDS of spent catalyst.

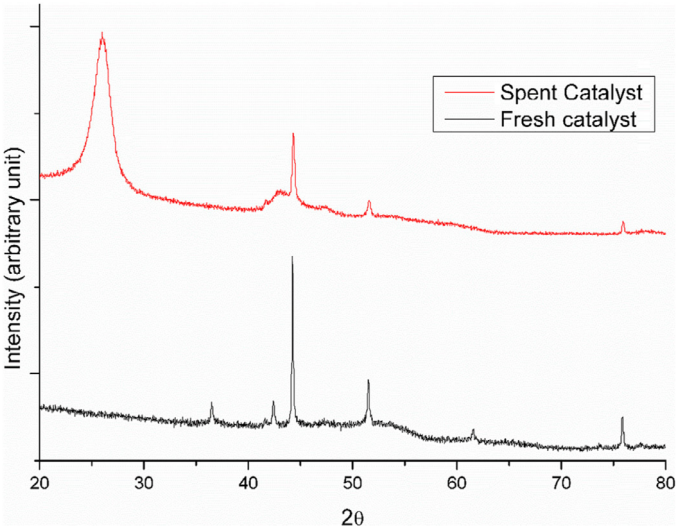

Fig. 6. HR-XRD of fresh and spent catalyst.

planes in carbon deposition. Both of these planes get sandwiched between the hexagonal primitive forms of carbon, which can be seen in Fig. 7b.

3.3. Adsorption studies

The adsorption studies performed with pH, concentration, dose and time was shown in Fig. 8. To check the adsorption efficiency pH may or may not significantly affect the removal of dye. Therefore, effect of pH with removal of Orange G dye was performed. The pH_{ZPC} of adsorbent (Co + Carbon) was found 8.1. The optimum pH for maximum removal of dye was observed at pH 2. With increase in pH from 2 to 4 the adsorption was decreased abruptly from 75% to 35%. The surface charge and level of ionization are influenced with pH. Due to anionic nature of Orange G dye and presence of several electronegative elements (O and S) with its functional group leads to variable adsorption efficiency with pH. It shows that pH has crucial role in adsorption for the removal of Orange G dye.

Batch experiment conducted for 120 minutes to find out the optimum contact time (Fig. 7). The experimental condition was kept as concentration of 30 ppm, pH = 2, agitation speed = 90 rpm, and adsorbent dose of 1 g/L. Orange G dye removal was found 76% within 10 minutes but 90.1% after 60 minutes. Initially, the swift removal of dye occurred but after 90 minutes, it achieved the equilibrium of adsorption. The prompt removal of dye at initial stage can be attributed to boundary layer diffusion and the presence of accessible vacant active sites at the surface of adsorbent. During completion of adsorption the intense competition between adsorbate molecules and transport of Orange G dye from external to internal sites makes it a slow process.

The effect of concentration (20 ppm to 60 ppm) was performed at optimum pH = 2 with 90 minutes contact time with adsorbent dose of 1 g/L. The percentage removal of dye was reduced with increase in concentration. It can be due to the reduction in number of dye molecules to available active sites ratio by the increase in concentration. Hence, active binding sites get covered resulted into diminished removal efficiency.

The adsorbent dose behaviour was analysed by variation of the adsorbent dose from 0.25 g/L to 2 g/L at pH = 2, stirring

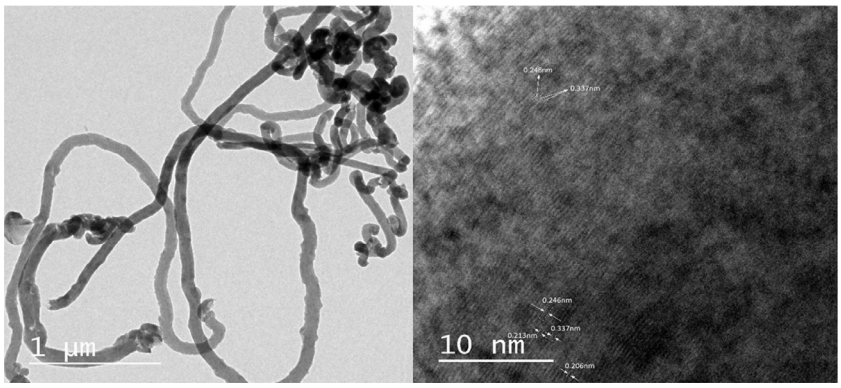

Fig. 7. TEM image of Co and carbon filament.

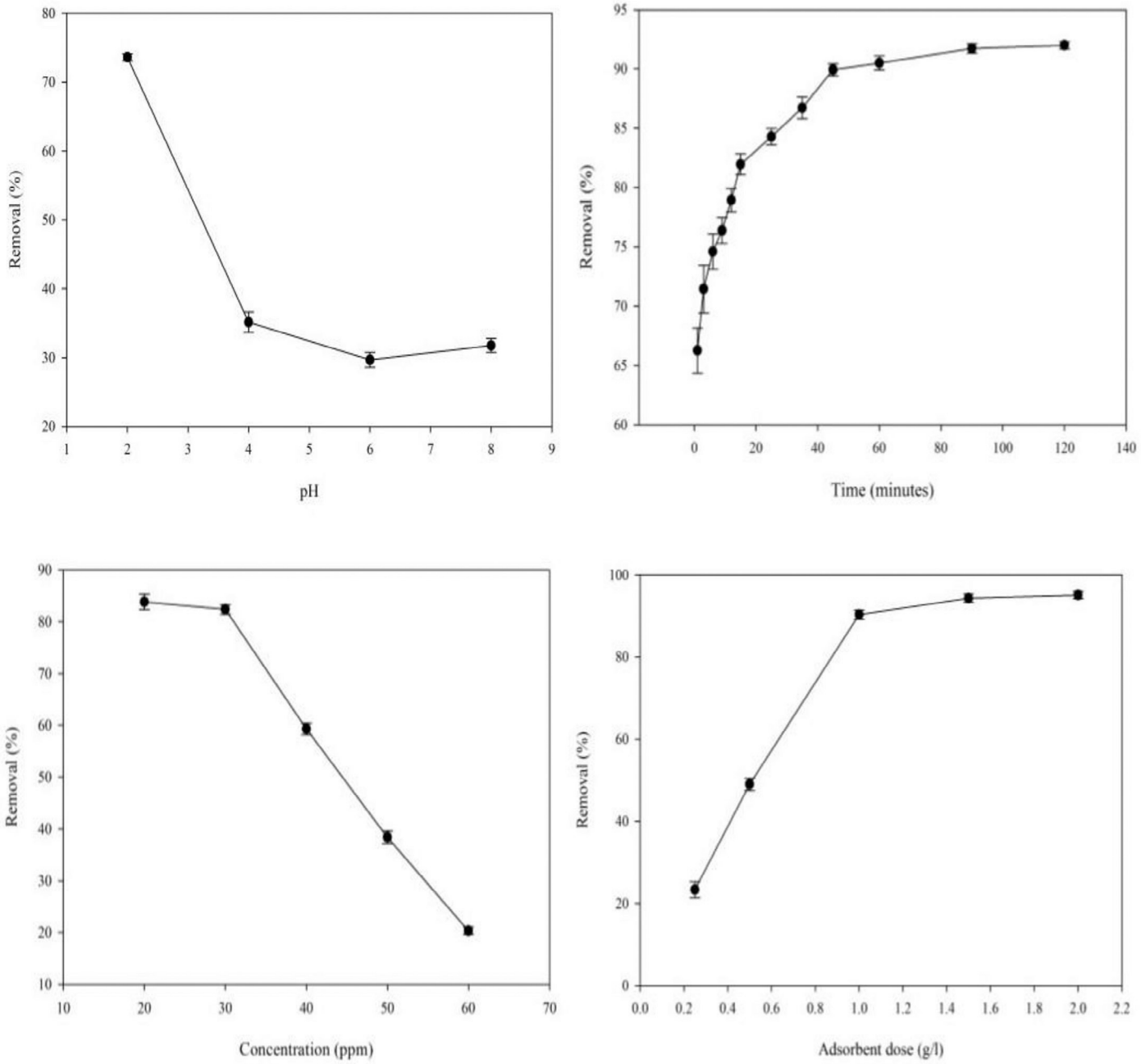

Fig. 8. Adsorption studies plots of removal (%) vs pH, time (minutes), concentration (ppm), adsorbent dose (g/l).

speed = 90 rpm. The increase in dose 0.25 g/L to 1 g/L has shown elevation in adsorption from 23% to 90.1% owing to elevation in the number of available active sites for adsorption. Moreover, increasing the dose from 1 g/L to 2 g/L has not shown significant increment in adsorption efficiency. It can be explained as higher number of unsaturated.

4. Conclusion

In this study, non noble Co metal catalyst predominantly in Co^0 state without any support was used for renewable hydrogen generation through ESR. It has been found that Cobalt in Co^0 state with (111) and (200) planes actively generates hydrogen with 96.5% selectivity and 100% ethanol conversion started at 723K temperature. The time on stream study also suggest the stability of Co for 19h in the absence of support in terms of H_2 selectivity. The absence of CoO state in spent catalyst occurred due to reduction of this state during ESR performance. The presence of Co metal at the tip of carbon nano filament was confirmed by SEM-EDS analysis of spent catalyst. It supports the carbon filament formation following tip growth phenomenon in Co metallic state. However, Co metal was also found in between the filaments. It suggests that it may follow Y-junction carbon growth or both ended carbon growth. It was also an interesting point that after the reaction, not a single co metal was found into 500–600 nm size. It may be due to separations of agglomerated cobalt particles (due to thermal treatment of $CoC_2O_4.2H_2O$) during carbonaceous deposition. The carbonaceous deposition used for Orange G dye removal has shown very high removal efficiency 552 mg/g at optimum parameter of pH = 2, contact time = 60 minute, concentration = 30 ppm, and dose = 0.05g. This adsorption capacity of the carbonaceous deposition was found without any surface modification or chemical treatment. This method gives a renewable cyclic approach for the production of hydrogen as energy carrier and waste water treatment. The adsorbate and adsorbent may have potential for further catalyst preparation through regeneration by oxidation. Overall, this study enlightens the path for further sustainable use of waste (Carbon + Co) for water pollution treatment.

Acknowledgements

The authors are thankful for Indian Institute of Technology (BHU) for providing financial assistance to the junior author (AK) and also for providing Institute Research Project.

References

[1] D. Bhatt, R. Mall, Surface water resources, climate change and simulation modeling, Aquat. Procedia 4 (2015) 730–738.
[2] S. Sharma, A. Roy, M. Agrawal, Spatial variations in water quality of river Ganga with respect to land uses in Varanasi, Environ. Sci. Pollut. Res 23 (2016) 21872–21882.
[3] J. Lin, L. Chen, C.K.S. Choong, Z. Zhong, L. Huang, Molecular catalysis for the steam reforming of ethanol, Sci. China Chem 58 (2015) 60–78.
[4] R. Ma, B. Castro-Dominguez, I.P. Mardilovich, A.G. Dixon, Y.H. Ma, Experimental and simulation studies of the production of renewable hydrogen through ethanol steam reforming in a large-scale catalytic membrane reactor, Chem. Eng. J. (2016), doi:10.1016/j.cej.2016.06.021.
[5] A. Al-Musa, M. Al-Saleh, Z.C. Ioakeimidis, M. Ouzounidou, I.V. Yentekakis, M. Konsolakis, et al., Hydrogen production by iso-octane steam reforming over Cu catalysts supported on rare earth oxides (REOs), Int. J. Hydrogen Energy 39 (2014) 1350–1363.
[6] C. Montero, A. Remiro, A. Arandia, P.L. Benito, J. Bilbao, A.G. Gayubo, Reproducible performance of a Ni/La_2O_3–αAl_2O_3 catalyst in ethanol steam reforming under reaction–regeneration cycles, Fuel Process. Technol 152 (2016) 215–222.
[7] G. Vari, L. Ovari, C. Papp, H.P. Steinruck, J. Kiss, Z. Konya, The interaction of cobalt with CeO_2(111) prepared on Cu(111), J. Phys. Chem. C 119 (2015) 9324–9333.
[8] H. Wang, Y. Liu, L. Wang, Y.N. Qin, Study on the carbon deposition in steam reforming of ethanol over Co/CeO_2 catalyst, Chem. Eng. J. 145 (2008) 25–31.
[9] J.M. Sun, A.M. Karim, D.H. Mei, M. Engelhard, X.H. Bao, Y. Wang, New insights into reaction mechanisms of ethanol steam reforming on Co-ZrO_2, Appl. Catal. B Environ 162 (2015) 141–148.
[10] A.R. Passos, L. Martins, S.H. Pulcinelli, C.V. Santilli, V. Briois, Effect of the balance between Co(II) and Co(0) oxidation states on the catalytic activity of cobalt catalysts for Ethanol Steam Reforming, Catal. Today 229 (2014) 88–94.
[11] Y.Z. Yue, F. Liu, L. Zhao, L.H. Zhang, Y. Liu, Loading oxide nano sheet supported Ni-Co alloy nanoparticles on the macroporous walls of monolithic alumina and their catalytic performance for ethanol steam reforming, Int. J. Hydrogen Energy 40 (2015) 7052–7063.
[12] R. Espinal, A. Anzola, E. Adrover, M. Roig, R. Chimentao, F. Medina, et al., Durable ethanol steam reforming in a catalytic membrane reactor at moderate temperature over cobalt hydrotalcite, Int. J. Hydrogen Energy 39 (2014) 10902–10910.
[13] G. Garbarino, P. Riani, M.A. Lucchini, F. Canepa, S. Kawale, G. Busca, Cobalt-based nanoparticles as catalysts for low temperature hydrogen production by ethanol steam reforming, Int. J. Hydrogen Energy 38 (2013) 82–91.
[14] R. Espinal, E. Taboada, E. Molins, R.J. Chimentao, F. Medina, J. Llorca, Cobalt hydrotalcite for the steam reforming of ethanol with scarce carbon production, RSC Adv 2 (2012) 2946.
[15] M. Domínguez, E. Taboada, E. Molins, J. Llorca, Ethanol steam reforming at very low temperature over cobalt talc in a membrane reactor, Catal. Today 193 (2012) 101–106.
[16] L. Chen, C.K.S. Choong, Z. Zhong, L. Huang, Z. Wang, J. Lin, Support and alloy effects on activity and product selectivity for ethanol steam reforming over supported nickel cobalt catalysts, Int. J. Hydrogen Energy 37 (2012) 16321–16332.
[17] B. Bayram, I.I. Soykal, D. von Deak, J.T. Miller, U.S. Ozkan, Ethanol steam reforming over Co-based catalysts: investigation of cobalt coordination environment under reaction conditions, J. Catal 284 (2011) 77–89.
[18] J. Llorca, P.R.R. de la Piscina, J.A. Dalmon, J. Sales, N.S. Homs, CO-free hydrogen from steam-reforming of bioethanol over ZnO-supported cobalt catalysts: effect of the metallic precursor, Appl. Catal. B Environ 43 (2003) 355–369.
[19] J. Llorca, Efficient production of hydrogen over supported cobalt catalysts from ethanol steam reforming, J. Catal 209 (2002) 306–317.
[20] M. Konsolakis, Z. Ioakimidis, T. Kraia, G. Marnellos, Hydrogen production by ethanol steam reforming (ESR) over CeO2 supported transition metal (Fe, Co, Ni, Cu) catalysts: insight into the structure-activity relationship, Catalysts 6 (2016) 39.
[21] H. Song, U.S. Ozkan, Changing the oxygen mobility in Co/Ceria catalysts by Ca incorporation: implications for ethanol steam reforming, J. Phys. Chem. A 114 (2009) 3796–3801.
[22] H. Song, B. Mirkelamoglu, U.S. Ozkan, Effect of cobalt precursor on the performance of ceria-supported cobalt catalysts for ethanol steam reforming, Appl. Catal. A Gen 382 (2010) 58–64.
[23] D. Gusain, S.N. Upadhyay, Y.C. Sharma, Adsorption of Orange G dye on nano zirconia: error analysis for achieving the best equilibrium and kinetic modeling, RSC Adv 4 (2014) 18755–18762.
[24] D. Gusain, S. Dubey, S.N. Upadhyay, C.H. Weng, Y.C. Sharma, Studies on optimization of removal of orange G from aqueous solutions by a novel nano adsorbent, nano zirconia, J. Ind. Eng. Chem 33 (2016) 42–50.
[25] G. Busca, U. Costantino, T. Montanari, G. Ramis, C. Resini, M. Sisani, Nickel versus cobalt catalysts for hydrogen production by ethanol steam reforming: Ni—Co–Zn–Al catalysts from hydrotalcite-like precursors, Int. J. Hydrogen Energy 35 (2010) 5356–5366.
[26] Y. Chen, Z. Shao, N. Xu, Ethanol steam reforming over Pt catalysts supported on $Ce_xZr_{1-x}O_2$ prepared via a glycine nitrate process, Energy Fuels 22 (2008) 1873–1879.
[27] S. Gunduz, T. Dogu, Hydrogen by steam reforming of ethanol over Co-Mg incorporated novel mesoporous alumina catalysts in tubular and microwave reactors, Appl. Catal. B Environ 168 (2015) 497–508.
[28] D. Dollimore, D. Griffiths, Differential thermal analysis study of various oxalates in oxygen and nitrogen, J. Therm. Anal 2 (1970) 229–250.
[29] Z. Ferencz, A. Erdohelyi, K. Baán, A. Oszkó, L. Óvári, Z. Kónya, et al., Effects of support and Rh additive on Co-based catalysts in the ethanol steam reforming reaction, ACS Catal 4 (2014) 1205–1218.
[30] S. Tuti, F. Pepe, On the catalytic activity of cobalt oxide for the steam reforming of ethanol, Catal. Lett 122 (2008) 196.
[31] F. Frusteri, S. Freni, V. Chiodo, L. Spadaro, O. Di Blasi, G. Bonura, et al., Steam reforming of bio-ethanol on alkali-doped Ni/MgO catalysts: hydrogen production for MC fuel cell, Appl. Catal. A Gen 270 (2004) 1–7.
[32] M. Li, X. Wang, S. Li, S. Wang, X. Ma, Hydrogen production from ethanol steam reforming over nickel based catalyst derived from Ni/Mg/Al hydrotalcite-like compounds, Int. J. Hydrogen Energy 35 (2010) 6699–6708.
[33] C. Wu, P.T. Williams, Hydrogen production from steam reforming of ethanol with nano-Ni/SiO2 catalysts prepared at different Ni to citric acid ratios using a sol–gel method, Appl. Catal. B Environ 102 (2011) 251–259.
[34] V. Nichele, M. Signoretto, F. Pinna, F. Menegazzo, I. Rossetti, G. Cruciani, et al., Ni/ZrO_2 catalysts in ethanol steam reforming: inhibition of coke formation by CaO-doping, Appl. Catal. B Environ 150–151 (2014) 12–20.
[35] J. Singh, S. Banerjee, D. Gusain, Y.C. Sharma, Equilibrium modelling and thermodynamics of removal of orange g from its aqueous solutions, J. Appl. Sci. Environ. Sanit 6 (2011) 317–326.
[36] A. Moisala, A.G. Nasibulin, E.I. Kauppinen, The role of metal nanoparticles in the catalytic production of single-walled carbon nanotubes – a review, J. Phys. Condens. Matter 15 (2003) S3011–S3035.
[37] H. Nakano, J. Nakamura, Carbide-induced reconstruction initiated at step edges on Ni(111), Surf. Sci 482–485 (Pt 1) (2001) 341–345.